II International Conference on Particle-based Methods - Fundamentals and Applications
PARTICLES 2011
E. Oñate and D.R.J. Owen (Eds)

A FULLY COUPLED 3D TRANSPORT MODEL IN SPH FOR MULTI-SPECIES REACTION-DIFFUSION SYSTEMS

S. ADAMI[a], X.Y. HU[a], N.A. ADAMS[a], E.M. RYAN[b] AND A.M. TARTAKOVSKY[b]

[a]Institute of Aerodynamics and Fluid Mechanics
Technische Universität München
85748 Garching, Germany
Corresponding author: stefan.adami@tum.de

[b]Computational Mathematics Technical Group
Pacific Northwest National Laboratory
Richland, WA 99352, USA

Key words: SPH, Porous media, Reaction-diffusion

Abstract. In this paper we present a fully generalized transport model for multiple species in complex two and three-dimensional geometries. Based on previous work [1] we have extended our interfacial reaction-diffusion model to handle arbitrary numbers of species allowing for coupled reaction models. Each species is tracked independently and we consider different physics of a species with respect to the bulk phases in contact. We use our SPH model to simulate the reaction-diffusion problem on a pore-scale level of a solid oxide fuel cell (SOFC) with special emphasize on the effect of surface diffusion.

1 INTRODUCTION

In the context of global warming a lot of effort has been focused on developing renewable and alternative energy sources that reduce the production of greenhouse gases. A promising alternative energy technology, which converts chemical energy to electrical energy is the cold combustion in fuel cells. Amongst various realizations of this technology, solid oxide fuel cells (SOFC) are of special interest as their working conditions at high temperatures enable the usage of a wide variety of fuels [7]. Degradation is a central issue in SOFCs, such as chromium poisoning, which arises from the chromium contained in the stainless steel which is typically used for the current collectors. This chromium reacts with air to form volatile chromium species that [8] migrate into the porous cathode and react with its surface. This so-called *chromium poisoning* has been shown to decrease the efficiency of the fuel cell dramatically and has to be controlled [6].

Ryan et al. [12] have developed a pore-scaled SPH model of a SOFC to investigate the reactive transport of chromium species in the cathode. Based on a multi-scale approach including a cell level model of the cathode, air channel and the current collector they determined the boundary conditions for the pore scale simulations. In their two-dimensional work they varied the reaction rates of oxygen and chromium and the working conditions of the fuel cell to study the deposition of chromium. They could reproduce qualitatively the species distributions in the cathode as compared to experimental findings [6] and show that their nonlinear competitive adsorption-desorption model is adequate to study the complex chromium poisoning.

In our current work we want to use the competitive adsorption-desorption model to simulate the chromium deposition in a realistic three-dimensional cathode. Different from the two-dimensional study of Ryan et al., here we cannot neglect surface diffusion in the porous material as this structure allows an interfacial connection throughout the entire domain and diffusion along the interface can alter the species dynamics strongly.

To simulate a multi-component reactive transport problem we have extended our SPH method for surfactant dynamics [1] to account for multiple species and coupled transport models. We have validated this method with analytical solutions for coupled transport-diffusion systems with different boundary conditions (Neumann, Dirichlet and Robin) and demonstrate the significance of surface diffusion for the species transport in a real porous cathode structure.

2 GOVERNING EQUATIONS

Briefly we recall the governing equations of the fluid and species dynamics in a porous structure in a very general form. From mass conservation we can formulate the continuity equation in the form

$$\frac{d\rho}{dt} = -\rho \nabla \cdot \vec{\mathbf{u}} \ , \tag{1}$$

where ρ, $\vec{\mathbf{u}}$ and t denote the density, the velocity vector and the time, respectively. The momentum equation in Lagrangian form with the pressure p, a bodyforce $\vec{\mathbf{g}}$ and the dynamic viscosity η is given by

$$\rho \frac{d\vec{\mathbf{u}}}{dt} = -\nabla p + \rho \vec{\mathbf{g}} + \nabla \eta \nabla \ . \vec{\mathbf{u}} \tag{2}$$

An advection-diffusion equation is used to describe the dynamics of a species α in a bulk phase l according to

$$\frac{dm_C^\alpha}{dt} = \int \nabla \mathbf{D}_\infty^\alpha \nabla C^\alpha \ dV - \int \dot{S_\Sigma}^\alpha \delta_\Sigma \ dV \ . \tag{3}$$

Here, m_C^α and C^α denote the mass and mass concentration of the species α in the bulk. Assuming isotropic bulk diffusion the diffusion tensor $\mathbf{D}_\infty{}^\alpha$ reduces to the scalar diffusion coefficient D_∞^α. Note that the bulk diffusion can vary for each species in different bulk

phases, i.e. the diffusion coefficient D_∞^α is a function of the species type α and the bulk phase where it is dissolved. The last term in (3) represents the transport of species α from/to the bulk phase to/from an interface it is in contact with. In continuous form the source term $\dot{S_\Sigma}^\alpha$ on the interface Σ is integrated in the domain via the surface delta function δ_Σ.

On the interface we account for surface diffusion and species transport via

$$\frac{dm_\Gamma^\alpha}{dt} = \int \nabla_s D_s^\alpha \nabla_s \Gamma^\alpha \delta_\Sigma \, dV + \int \dot{S_\Sigma}^\alpha \delta_\Sigma \, dV \ , \tag{4}$$

where m_Γ^α, Γ^α and D_s^α are the mass and mass concentration of species α on the interface Σ and the surface diffusion coefficient (again assuming isotropic surface diffusion). Note, the surface gradient operator ∇_s can be written as $(\mathbf{I} - \vec{\mathbf{n}} \otimes \vec{\mathbf{n}}) \nabla$, which will be used later. The second term in (4) is equivalent to the source mass flux in the species balance equation in the bulk phase (3) to ensure mass conservation of each species.

The surface transport model in a very general form is given by

$$\dot{S_\Sigma}^\alpha = f\left(C^1, C^2, ..., C^\alpha, \Gamma^1, \Gamma^2, ..., \Gamma^\alpha\right) \ . \tag{5}$$

Here, the source term $\dot{S_\Sigma}$ is a function of the surface concentrations Γ and the bulk concentrations C adjacent to the interface of all species α in the system. We implemented this general formulation to include arbitrarily complex transport models starting from the most simple no flux condition $\dot{S_\Sigma}^\alpha = 0$ up to coupled competitive reaction models such as the Langmuir model [14].

3 NUMERICAL METHOD

Generally, the equations of motion for a Lagrangian fluid element can be integrated in time with the SPH method as presented in [10]. In the weakly-compressible approach the unknown pressure in the fluid phase is calculated from the density via an equation of state in the form

$$p = p_0 \left(\frac{\rho}{\rho_0}\right)^\gamma , \tag{6}$$

where the reference pressure p_0 and density ρ_0 together with the exponent γ are chosen according to a scale analysis to limit the maximum density variation, see [11]. As we do not evolve the flow quantities of the fluid in this work we do not further explain the details of our flow solver but concentrate on the species model. The simplification of neglecting advection to study the competitive reaction-diffusion problem in a porous structure is justified by the work of [12], who showed that advection processes in the cathode are insignificant for the chromium poisoning.

We discretize the domain of interest with Cartesian particles with an equidistant spacing of Δx. Consequently, the volume of a particle i is $V_i = \Delta x^n$ with n denoting the number of dimensions. The quintic spline kernel [11] is used as smoothing function W

with a cutoff radius $r_c = 3h$, where the smoothinglength h is set to the initial particle distance. Following the multi-phase model of [9], we introduce a color function c that defines if a particle i belongs to a phase l ($c_i^l = 1$) or not ($c_i^l = 0$). Using this color function phase interfaces are defined implicitly as the color gradient ∇c is non-vanishing only in a transition band of thickness r_c along the interface. Within this transition band, the governing equations for the surface dynamics of the species are solved locally for each individual particle.

As the interface singularity is represented by a continuous surface delta-function (here the magnitude of the color-gradient function $|\nabla c|$ is used as δ_Σ) every particle in the narrow band along an interface contributes to the interface area by

$$A_i = |\nabla c_i| \, V_i \ . \tag{7}$$

Correspondingly, every interface particle carries a fraction of the mass of species α accumulated on the interface $m_{\Gamma_i}^\alpha = \Gamma_i^\alpha A_i$. As the interface singularity is discretized by a transition band of finite thickness, we can use the derivations of [3] and solve the surface diffusion equation in continuous form for every interface particle as

$$\frac{d\Gamma_i^\alpha}{dt} = \frac{1}{|\nabla c_i|} \nabla \cdot \left[\left(\mathbf{I} - \vec{\mathbf{n}}_\mathbf{i} \otimes \vec{\mathbf{n}}_\mathbf{i} \right) D_s^\alpha \nabla \Gamma_i^\alpha \, |\nabla c_i| \right] \ . \tag{8}$$

The normal direction at the interface $\vec{\mathbf{n}}_\mathbf{i}$ is found from an averaging of the normalized color-gradient vectors of neighboring interface particles. Finally, the rate of change of the interfacial mass $m_{\Gamma_i}^\alpha$ due to surface diffusion is obtained by

$$\frac{dm_{\Gamma_i}^\alpha}{dt} = \sum_j \left(\lambda_i^\alpha V_i^2 + \lambda_j^\alpha V_j^2 \right) \nabla W \left(\vec{\mathbf{x}}_i - \vec{\mathbf{x}}_j \right) \ . \tag{9}$$

The summation is over all neighboring particles j that contribute to the interface and λ_i^α is the flux of species α projected in tangential surface direction at particle i ($\lambda = (\mathbf{I} - \vec{\mathbf{n}}_\mathbf{i} \otimes \vec{\mathbf{n}}_\mathbf{i}) \, D_s^\alpha \nabla \Gamma^\alpha \, |\nabla c|$). At the fringes of the transition band the surface gradient of a species concentration cannot be calculated with a general SPH gradient formula as the contributing interface particles do not provide full support for the summation. As a remedy, we can approximate the gradient on the interface by a summation only with interface particles as given by

$$\nabla \Gamma_i^\alpha = \frac{n \sum_j \left(\Gamma_i^\alpha - \Gamma_i^\alpha \right) \nabla W_{ij}}{\sum_j r_{ij} \frac{\partial W}{\partial r i j}} \tag{10}$$

with $r_{ij} = |\vec{\mathbf{x}}_i - \vec{\mathbf{x}}_j|$. For details of the derivation and accuracy of this form we refer to [2].

The evolution of the surface mass of a species due to exchange with the bulk phase for each interface particle is simply $dm_{\Gamma_i}^\alpha / dt = \dot{S}_\Sigma{}^\alpha \, |\nabla c_i| \, V_i$. The surface concentration is

updated in time by

$$\Gamma_i^\alpha = \frac{\sum_j m_{\Gamma_j}^\alpha W_{ij}}{\sum_j A_j W_{ij}} \ , \tag{11}$$

where the summation is performed over all neighboring interface particles. This additional averaging step is required as a simple local estimation could cause numerical instabilities due to very small interfacial contributions of particles close to the fringes of the interfacial transition band.

The presented model is based on a so-called two-sided physics assumption, i.e. the transport and diffusion phenomena are solved numerically on a layer adjacent to the interface of both phases. There are situations where one phase cannot dissolve a species but the surface transport model includes desorption of surface material to the other bulk phase. Then, we apply some special mapping techniques to ensure exact conservation of the species and to consider the total interfacial area. Further information of this special computational aspect can be found in [1]. A similar model for the one-sided problem has been proposed and validated in [13] for reactive transport problems with surface reactions.

The SPH approximation of the bulk diffusion equation in conservative form can be expressed as

$$\frac{dm_{C_i}^\alpha}{dt} = \sum_j \frac{2D_{\infty i}^\alpha D_{\infty j}^\alpha}{D_{\infty i}^\alpha + D_{\infty j}^\alpha} \left(V_i^2 + V_j^2\right) \frac{C_i^\alpha - C_j^\alpha}{r_{ij}} \frac{\partial W}{\partial r_{ij}} \ . \tag{12}$$

Note that the inter-particle averaged diffusion coefficient in (12) satisfies the no-flux condition between two particles if the species is insoluble in one of the phases. Additionally, the bulk species mass of a particle close to an interface changes due to the adsorption and desorption at the interface as $dm_{C_i}^\alpha/dt = -\dot{S}_{\Sigma_i}^{\ \alpha} \left|\nabla c_i\right| V_i$.

The anti-symmetry of the discretized transport equations in the bulk phase (12) and on the interface (9) on the local particle-interaction level ensures exact global species mass conservation.

We have presented a method to simulate multi-species reaction-diffusion problems on complex geometries with SPH. Generally, the equations hold for arbitrary numbers of species α each following different physical models. But with increasing variety the computational effort increases as for every species the transport model coefficients such as surface diffusivity or adsorption constants have to be defined separately for every interface combination and bulk phase. So far, we have not yet specified a transport model for the source term $\dot{S}_\Sigma^{\ \alpha}$ in the species evolution equation as any functional form including the local bulk and surface concentrations can be used. We present the employed transport models in the next section where we show some validation cases. Finally, we study the coupled species dynamics on a realistic three-dimensional porous structure of a SOFC cathode.

4 VALIDATION

We solve the diffusion problem in a hollow cylinder with different boundary flux conditions to validate our model. A sketch of the problem is given in Fig. 1. At the outer radius R_o the species concentration is set to C_0 for all times and at the inner radius R_i different boundary flux conditions are tested. Initially, the concentration in the hollow cylinder is $C(t = 0) = 0$. The inner and outer radii are $R_i = 1$ and $R_o = 2$ and we discretize the geometry with Cartesian SPH particles with $\Delta x = 0.05$, i.e. we use 20 particles in radial direction. We compare our results with the analytical solution for bulk diffusion in a hollow cylinder with a flux boundary condition given by [5].

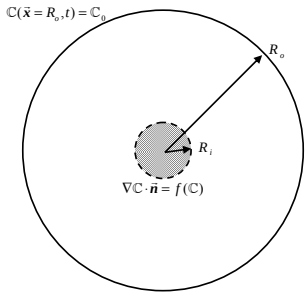

Figure 1: Sketch of the hollow cylinder problem.

4.1 Neumann boundary condition

At first we apply a Neumann boundary condition at the inner radius

$$D\nabla C|_{R_i} \cdot \vec{\mathbf{n}} = q_0 \tag{13}$$

with the constant flux q_0. When we rewrite the boundary condition in terms of a transport model to/from the interface, the source term in the species evolution equation is $\dot{S_\Sigma} = q_0$.

Fig. 2 shows spatial concentration profiles over time in the bulk phase with $D = 1$. In this special case we set $q_0 = 0$, i.e. a no-flux boundary condition at the inner radius. The agreement with the analytic result is good and the accuracy increases with resolution.

Now we use a constant boundary flux $q_0 = 0.1$ to validate the mass transport at an interface. Again, good agreement and convergence is found when comparing the simulations with the reference solution, see Fig. 3. Not shown here, we also monitored the mass accumulated at the interface due to the boundary flux and found exact global conservation for our transport model.

4.2 Robin boundary condition

Now we test a more complex linear Robin boundary condition of the form

$$D_\infty \nabla C \cdot \vec{\mathbf{n}} = K\,(C - C_{eq}) \tag{14}$$

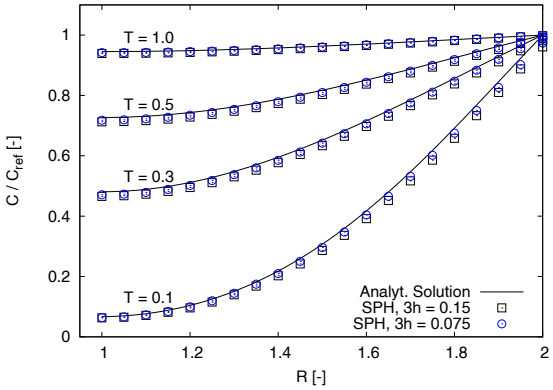

Figure 2: Radial concentrations over time in the hollow cylinder for the no-flux boundary condition at R_i.

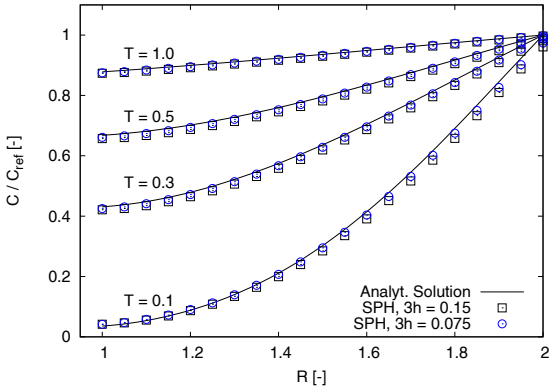

Figure 3: Radial concentrations over time in the hollow cylinder with a Neumann boundary condition at R_i.

with the equilibrium concentration C_{eq} and a reaction rate K. In this case we use $D = 0.1$, $C_{eq} = 0.5$ and $K = 1$. The radial concentration profiles over time are shown in Fig. 4.

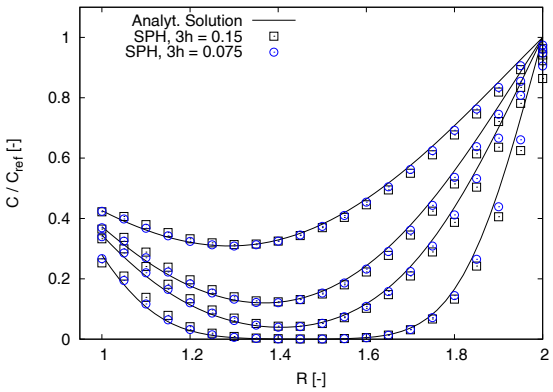

Figure 4: Radial concentrations over time in the hollow cylinder with a linear Robin boundary condition at R_i.

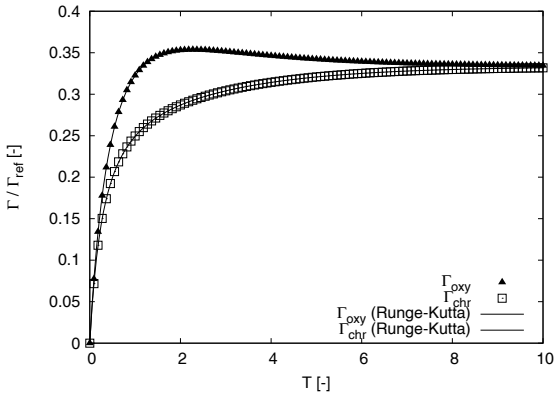

Figure 5: Temporal surface concentration profile for two species *oxy* and *chr* for a competitive adsorption model.

As the initial bulk concentration is zero, according to the boundary condition (14) a negative flux injects mass to the bulk phase at the inner radius. Consequently, the concentration profile is different from the previous diffusive profiles as species material is transported to the inner regions by the boundary flux and not only via diffusion from the outer radius. At very late times, the concentration at the inner interface approaches the equilibrium value of the Robin condition C_{eq}.

4.3 Competitive adsorption-desorption model

So far we have simulated uncoupled problems, i.e. each species is independent of the other ones. Now we use the modified Langmuir model [14] to simulate competitive adsorption of two components. The non-linear source terms for the two species *oxy* and *chr* are

$$\dot{S_\Sigma}^{oxy} = k_1^{oxy} C_\infty^{oxy} \left[1 - \Gamma^{oxy} - \Gamma^{chr}\right]^2 - k_2^{oxy} \left(\Gamma^{oxy}\right)^2 \tag{15}$$

$$\dot{S_\Sigma}^{chr} = k_1^{chr} C_\infty^{chr} \left[1 - \Gamma^{oxy} - \Gamma^{chr}\right]^3 - k_2^{chr} \left(\Gamma^{chr}\right)^3 \ . \tag{16}$$

We simulate the adsorption process from a bulk phase to a circular interface with radius $R = 1$. We assume diffusion to be much larger than the surface reaction rates, i.e. the bulk concentrations $C_\infty^{oxy} = 1$ and $C_\infty^{chr} = 1$ are both constant in time. For simplicity we set all reaction constants k_1 and k_2 to unity and use the same discretization as in the previous examples.

From our parameter setup we find an equilibrium for both species concentrations at

$$\Gamma^{oxy} = \Gamma^{chr} = \frac{1}{3} \tag{17}$$

where the surface reaction is balanced and a steady-state is reached. In Fig. 5 we show the temporal evolution of the averaged surface concentrations for both species. We compare our results with a quasi-onedimensional high resolution finite-difference calculation using a fourth order Runge-Kutta integration scheme and very good agreement is found. In the beginning, adsorption of species *oxy* is faster than species *chr* and an overshoot of the equilibrium condition occurs. Later, both components reach the steady equilibrium state and the net surface flux is zero.

5 POROUS STRUCTURE

We have demonstrated the validity of our method to simulate complex surface transport problems on curved interfaces in two dimensions. Now we want to study a more realistic three-dimensional reaction-diffusion problem in a porous structure as it occurs in a SOFC cathode. For that purpose we take a pixelmap of a section of a real cathode structure provided by the Pacific Northwest National Laboratory and discretize the pores and the air phase with different types of particles, see the red (pores) and blue (air) particles in Fig. 6.

Using the color-function gradient between the two phases to determine the interface position, we can reconstruct the surface of the pores and simulate the interfacial diffusion of a scalar species coupled with bulk transport. Fig. 7 shows the reconstruction of the interface using our SPH discretization of the problem. The non-dimensional size of the geometry is $32 \times 32 \times 16$ and we have used a particle spacing of $\Delta x = 0.25$. Thus a total of 1,048,576 particles is used.

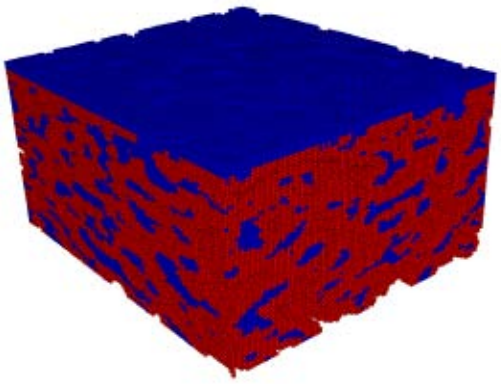

Figure 6: Discretization of a section of a real cathode filled with air with SPH particles.

Figure 7: Interface reconstruction of the porous cathode from the SPH discretization.

As we are interested in the impact of surface diffusion, we do not simulate an entire fuel cell with an air channel, current collector, anode and cathode but study the species dynamics in a section of the cathode to estimate time scales and the influence of reaction rates and surface diffusion on the distribution of a species in the cathode. Then we can use these results to improve continuous coarse-grid models for porous media and study the depositioning of chromium in a real cathode.

In this work we compare three simulations with an isolated species at different diffusion rates to demonstrate that surface diffusion can strongly change the dynamics of the *poisoning*. The Langmuir adsorption-desorption model given by

$$\dot{S_\Sigma} = k_1 C \left(\Gamma_{max} - \Gamma\right) - k_2 \Gamma \tag{18}$$

is used for the surface transport with the parameter $k_1 = 1.0$, $k_2 = 0.2$ and $\Gamma_{max} = 1.0$. At the top layer we define the bulk concentration of chromium $C_\infty = 1.0$, constant in time. We impose symmetry boundary conditions in x and y direction as periodicity cannot be applied to a heterogeneous porous structure. Also the flux of species along the sidewise boundaries was shown to be marginal, hence negligible [12] which verifies the symmetry assumption. The bottom of the cathode section is impermeable for chromium and we use a no-flux boundary condition there.

Table 1 shows the parameters for the surface and bulk diffusion of our simulations. *Case 1* is dominated by a strong bulk diffusion, in *Case 2* we amplified the surface diffusion and *Case 3* is used as a reference result to estimate the effect of the two variations.

In Fig. 8 - 10 snapshots of the three simulations at $T = 8$ show a section of the interface and a slice through the bulk phase to show the surface concentration and the bulk concentration. The colors in the figures show the quantities from blue to red in the range of $\Gamma = 0 - 0.833$ and $C = 0 - 1$, respectively.

Table 1: Diffusion coefficients for the three cases.

	Case 1	*Case 2*	*Case 3*
D_s	0.1	1.0	0.1
D_∞	10.0	1.0	1.0

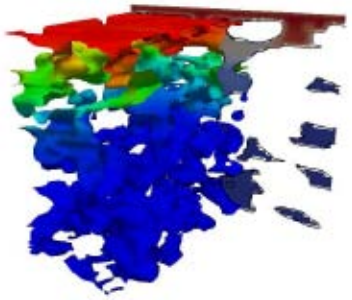

Figure 8: Surface and bulk concentration for *Case 1*

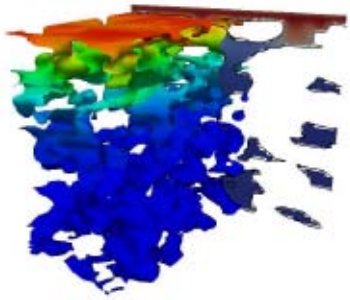

Figure 9: Surface and bulk concentration for *Case 2*

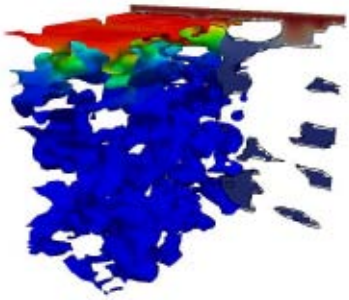

Figure 10: Surface and bulk concentration for *Case 3*

From these figures we see immediately the influence of bulk diffusion on the species distribution in the gas phase. The penetration depth of chromium in the bulk (Fig. 8) is larger than for the other cases. Interestingly, the surface concentration distribution is similar for *Case 1* and *Case 2* although the diffusion rates are inverse. To further analyse the results we postprocessed the concentration profiles and calculated average interface and bulk concentrations in small slices along the z-axis. Of course diffusion in the porous media is not uniform and not quasi-onedimensional in the z-direction, but from the averaged profiles we can better interpretate the results and describe qualitatively the effect of different parameter.

The averaged bulk concentration profiles in the z-direction at $T = 8$ for the three different cases are shown in Fig. 11. At the upper boundary at $z = 16$ the concentration is equal to the reference value and for the high bulk diffusivity the biggest amount of chromium mass is deposited into the porous structure. Correspondingly we show the averaged surface concentration in slices along the z-axis for all cases in Fig. 12. As a reference, we have also plotted the equilibrium surface concentration for the reference bulk concentration obtained from

$$\Gamma_{eq} = \frac{k_1 \Gamma_{max} C_\infty}{k_1 C_\infty + k_2} \ . \tag{19}$$

Close to the upper boundary, the surface concentration has already reached the equilibrium value and remains constant in time. The dots in this figure show the profile of the equilibrium surface concentration calculated from (19) using the local averaged bulk con-

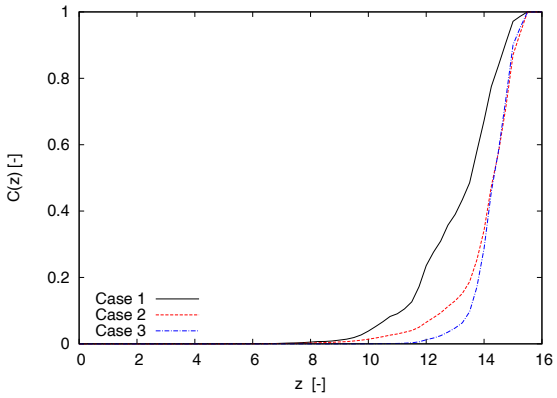

Figure 11: Averaged bulk concentration profiles in z-direction in the air phase filling the porous cathode.

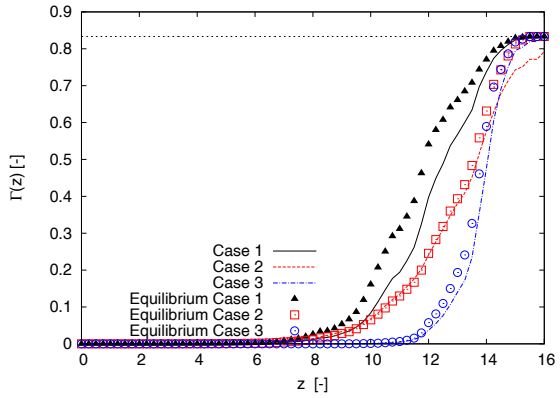

Figure 12: Averaged interfacial species concentration in z-direction of the porous structure.

centrations. Comparing the actual local profile and the theoretical equilibrium profile for *Case 1* we see that diffusion rates are much faster compared to the transport to the surface. Thus, the surface concentration in lower regions did not yet achieve the equilibrium condition as the adsorption rate is too small.

Moreover we want to emphasize that the two bulk concentrations of *Case 2* and *Case 3* differ considerably although the bulk diffusion coefficient is equal for both setups. This effect can be explained together with the surface concentration profiles and the Langmuir model. Looking at *Case 3*, the surface concentration profile coincides with the calculated equilibrium profile. That means chromium diffuses slowly through the bulk phase and almost instantaneously the surface reaction is in equilibrium with the bulk phase.

The bulk diffusion in *Case 2* is equivalent with *Case 3*, but much more material is already transported to the air phase in the cathode and the averaged bulk concentration profile in Fig. 11 is higher. This material comes from the desorption of chromium from the interface. The high surface diffusivity transports chromium along the interface into the structure. Consequently, the surface concentration gradient is smoothed stronger and even at the upper boundary the interface equilibrium condition is not yet reached. In addition, desorption takes place lower in the structure since the interface is oversaturated according to (19) and chromium occurs in a depth where pure bulk diffusion could not yet transport material.

6 CONCLUSION

We have presented a fully coupled multi-species SPH model considering the effect of surface diffusion, surface reaction and bulk diffusion. The validation against analytical and high-resolution results shows very good agreement and convergence of our method is proved. We used our method to simulate the complex interaction of surface diffusion, reaction and bulk diffusion in a three-dimensional porous structure of a real cathode of

a fuel cell and highlight the deposition of chromium into the cathode via surface diffusion. In future work we want to explore a more complex coupled two-species transport model to represent the competitive species dynamics of oxygen and chromium and use more realistic boundary conditions such as prescribed flux conditions and concentration dependent reaction rates.

ACKNOWLEDGMENT

The corresponding author gratefully acknowledges the support of the TUM Graduate School at the Technische Universität München and the support of the German Research Foundation (DFG - Deutsche Forschungsgesellschaft) for funding this work within project AD 186/6-1. We also want to thank John Biddiscombe (CSCS, Swiss National Supercomputing Centre, Switzerland) for the postprocessing software *pv-meshless* [4].

REFERENCES

[1] S. Adami, X.Y. Hu, and N.A. Adams. A new surface-tension formulation for multi-phase SPH using a reproducing divergence approximation. *J. Comput. Phys.*, 229(13):5011–5021, 2010.

[2] S. Adami, X.Y. Hu, and N.A. Adams. A conservative SPH method for surfactant dynamics. *J. Comput. Phys.*, 229(5):1909 – 1926, 2010.

[3] M. Bertalmío, L.T. Cheng, S. Osher, and G. Sapiro. Variational problems and partial differential equations on implicit surfaces. *J. Comput. Phys.*, 174(2):759–780, December 2001.

[4] J. Biddiscombe, D. Graham, and P. Maruzewski. Visualization and analysis of SPH data. *ERCOFTAC Bulletin*, 76:9–12, 2008.

[5] H.S. Carslaw and J.C. Jaeger. *Conduction of heat in solids*, volume 1. Oxford Univ. Press, New York, 1959.

[6] T. A. Cruse, B. J. Ingram, D. J. Liu, and M. Krumpelt. Chromium reactions and transport in solid oxide fuel cells. *ECS Transactions*, 5(1):335–346, 2007.

[7] K. Hayashi, O. Yamamoto, and H. Minoura. Portable solid oxide fuel cells using butane gas as fuel. *Solid State Ionics*, 132(3-4):343–345, July 2000.

[8] K. Hilpert, D. Das, M. Miller, D. H. Peck, and R. Weiß. Chromium vapor species over solid oxide fuel cell interconnect materials and their potential for degradation processes. *J. Electrochem. Soc.*, 143(11):3642–3647, 1996.

[9] X. Y. Hu and N. A. Adams. A multi-phase SPH method for macroscopic and mesoscopic flows. *J. Comput. Phys.*, 213(2):844–861, 2006.

[10] J. J. Monaghan. Smoothed particle hydrodynamics. *Reports in Progress in Physics*, 68(8):1703–1759, 2005.

[11] J.P. Morris, P.J. Fox, and Y. Zhu. Modeling low reynolds number incompressible flows using SPH. *J. Comput. Phys.*, 136(1):214–226, 1997.

[12] E. M. Ryan, A. M. Tartakovsky, and C. Amon. A novel method for modeling neumann and robin boundary conditions in smoothed particle hydrodynamics. *Comput. Phys. Comm.*, 181(12):2008 – 2023, 2010.

[13] E.M. Ryan, A.M. Tartakovsky, K.P. Recknagle, M.A. Khaleel, and C. Amon. Pore-scale modeling of the reactive transport of chromium in the cathode of a solid oxide fuel cell. *Journal of Power Sources*, 196(1):287 – 300, 2011.

[14] L. D. Schmidt. *The engineering of chemical reactions*. Oxford University Press, New York, 1998.